CrystEngComm

RSC Publishing

PAPER

View Article Online
View Journal | View Issue

Cite this: *CrystEngComm*, 2013, **15**, 5561

Bromoperoxidase mimic as catalysts for oxidative bromination—synthesis, structures and properties of the diversified oxidation state of vanadium(III, IV and V) complexes with pincer *N*-heterocycle ligands†

Chen Chen,[b] Qiao Sun,[c] Dong-Xue Ren,[b] Rui Zhang,[b] Feng-Ying Bai,*[a] Yong-Heng Xing*[b] and Zhan Shi[d]

Novel oxovanadium complexes $(VO)_2$(bpz*T-O) (**1**), VO(bpz*eaT)$(SCN)_2$ (**2**), V_2(bpz*eaT)$_2$(μ_2-C_2O_4)(C_2O_4)$_2$ (**3**), [VO(SO_4)(bpz*P)(H_2O)]·H_2O (**4**) and VO(SO_4)(bpz*P-Me)(H_2O) (**5**) (bpz*T-O: 4,6-bis(3,5-dimethylpyrazol-1-yl)-1,3,5-triazin-2-olate, bpz*eaT: 2,4-bis(3,5-dimethyl-1*H*-pyrazol-1-yl)-6-diethylamino-1,3,5-triazine, bpz*P: 2,6-bis(5-methyl-pyrazol-3-yl)pyridine, bpz*P-Me: 2,6-bis(1,5-dimethyl-pyrazol-3-yl)pyridine), were synthesized by the reaction of $V_2(SO_4)_3$–$VOSO_4$–VO(acac)$_2$ and various pincer *N*-heterocyclic ligands with solution or hydrothermal methods. The structures of all the complexes were characterized by elemental analysis, IR and UV-vis spectroscopy and single-crystal diffraction analysis. Furthermore, thermogravimetric analyses (TG) and quantum chemistry calculations were also performed. Structural analyses reveal that the vanadium atom has a distorted trigonal bipyramidal geometry with a N_3O_2 donor set in **1**; distorted octahedral geometry in **2**, **4** and **5** with donor sets of N_5O, N_3O_3 and N_3O_3, respectively; a distorted pentagonal bipyramidal geometry with a N_3O_4 donor set in **3**. In addition, the five new complexes with abundant intro- and inter-hydrogen bonding interactions exhibited bromination catalytic activity in a single-pot reaction of the conversion of phenol red to bromophenol blue in a mixed solution of H_2O–DMF at a constant temperature of 30 ± 0.5 °C with a buffer solution of NaH_2PO_4–Na_2HPO_4 (pH = 5.8), indicating that they can be considered as a potential functional model of bromoperoxidase.

Received 7th March 2013, Accepted 8th May 2013

DOI: 10.1039/c3ce40410b

www.rsc.org/crystengcomm

Introduction

The interest in the coordination chemistry of vanadium has increased in the last few decades because of its catalytic and biological importance.[1–7] Besides the insulin-enhancing activity of oxidovanadium(V) and oxidovanadium(IV) compounds,[8,9] vanadium haloperoxidases (VHPO)[3,10,11] are enzymes capable of catalyzing the oxidative bromination of a variety of organic substrates. Thereinto, the crystal structure of the vanadium bromoperoxidase (V-BrPO) from *Ascophyllum nodosum* shows that the central vanadium is covalently linked to the N^ε of the imidazolyl moiety of a histidine and through extensive hydrogen bonding to a variety of amino acid side chains (Arg, His, Ser, Lys) and interstitial water in the proximity of the active centre.[12,13] This determination of vanadium in the active sites of biological systems of bromoperoxidase and the recognition of its environment has increased the interest in vanadium complexes with organic ligands for mimicking the biological activity in natural systems. Oxidovanadium(IV) and dioxovanadium(V) complexes with N-, O- and S-donor chelating ligands have been studied for their potential in insulin-mimetic effects,[14] tumor growth inhibition and prophylaxis against carcinogenesis,[15] inhibiting several enzymes, including phosphatases, ATPases, nucleases, kinases[16] as well as the antimicrobial activity against Mycobacterium tuberculosis.[17] In particular, the application study of oxidovanadium complexes in oxidation and oxotransfer catalysis has recently attracted more attention, with various organic substrates being oxidized by peroxides in the presence of vanadium or dioxovanadium(V) complexes.[18,19]

In order to get a better understanding of the catalytic function mechanism of V-BrPO, to determine the role of

---

[a] *College of Life Science, Liaoning Normal University, Dalian 11602, P. R. China*
[b] *College of Chemistry and Chemical engineering, Liaoning Normal University, Huanghe Road 850#, Dalian 116029, P. R. China.*
E-mail: xingyongheng2000@163.com; Tel: +86-0411-82156987
[c] *ARC Centre of Excellence for Functional Nanomaterials, Australian Institute for Bioengineering and Nanotechnology, the University of Queensland, Brisbane, Australia*
[d] *State Key Laboratory of Inorganic Synthesis and Preparative Chemistry, College of Chemistry, Jilin University, Changchun 130012, P. R. China*

† Electronic supplementary information (ESI) available: Tables of atomic coordinates, isotropic thermal parameters and complete bond distances and angles. CCDC 893011 for **1**, 893015 for **2**, 893012 for **3**, 893013 for **4** and 893014 for **5**. For ESI and crystallographic data in CIF or other electronic format see DOI: 10.1039/c3ce40410b

vanadium and to explore the relationship between the structure and catalytical activity, it is necessary to synthesize a series of vanadium complexes containing oxygen and nitrogen donors as a functional model for V-BrPO.[10,11] A variety of ligands that yield active functional model systems for V-BrPO, including Schiff base ligands,[20] poly(pyrazolyl)borates[21] and so on, have so far been well developed in the coordination chemistry of vanadium. In the mean time, in our group, vanadium haloperoxidases functional model complexes with O-, N- or S-donor ligands have been tested for their bromination catalytic reaction activity in a single-pot reaction of the conversion of phenol red to bromophenol blue. This reaction is considered to have some important strong points: (i) the starting phenol red is catalyzed by H_2O_2 to the corresponding bromophenol blue, as observed by the immediate color change of the reaction; (ii) the low toxicity of KBr; (iii) there are no side reactions in the process, *etc*. To our knowledge, the study of synthesis, structure and catalytic activity of some oxidovanadium complexes with pincer *N*-heterocycle ligands is still rare. In addition, it is significant to further expand and apply other organic bromide reactions in industry because molecular bromine is a favorable agent for the synthesis of brominated organic compounds but it is corrosive and toxic, and moreover, the transport, storage and handling of bromine therefore requires strict safety standards in traditional industry.[22] By checking the catalytic function and various structures of oxidovanadium complexes, we have found that oxidovanadium complexes with pincer *N*-heterocycle ligands could possess better catalytic activity than other oxidovanadium complexes.

In recent years, pyrazole and its derivatives have been widely used in coordination chemistry owing to the good coordination ability of heterocyclics containing nitrogen atoms. Some complexes with pyrazolyl derived ligands have attracted considerable attention in catalysis, biomimetics, ion exchange and photophysical properties areas. As nitrogen containing heterocycles, pyrazolyl–triazine and bis(pyrazolyl)–pyridine ligands are two significant branches of pyrazole derivatives which have received great interest recently due to the fact that they are straightforward to synthesize and in particular, those substituted at the 3, 4 and 5-position on the pyrazolyl moiety are also readily accessible. In addition, they can bind to both low- and high-oxidation state metal ions, generally in a tridentate fashion.[23] In general, for pyrazolyl–triazine ligands, there are mainly two types that will be used in this work, as depicted in Scheme 1a, namely, 2,4,6-tri(3,5-dimethylpyrazol-1-yl)-1,3,5-triazine (L^1) and 2,4-bis(3,5-dimethyl-1*H*-pyrazol-1-yl)-6-diethylamino-1,3,5-triazine (L^2). The triazine ring is a particular aromatic moiety with a very strong electron-deficient character that allows for the formation of π–π stacking and anion–π interactions.[24] Furthermore, this ring contains three nitrogen atoms that can give rise to hydrogen bonds and can also coordinate to metal ions, such as tridentate terpyridine-like, bidentate bipyridine-like, mixed tridenate and bidentate types and bis-bipyridine-like.[25] For bis(pyrazolyl)pyridine derivative ligands, there are also mainly two types, as depicted in Scheme 1b. Compared with type i, type ii can display more coordinated sites and produce various complexes with different coordination modes easily.[26] To the best of our knowledge, many transition metal complexes with type ii ligands have been studied in recent decades[26a,b] but only a few kinds of coordination complexes with the 2,6-bis(5-methyl-1*H*-pyrazol-3-yl)pyridine (L^3) ligand have been synthesized and in particular, oxidovanadium complexes have not been reported up to now. Furthermore, there is also much less research of complexes with the 2,6-bis(1,5-dimethyl-pyrazol-3-yl)pyridine (L^4) ligand.

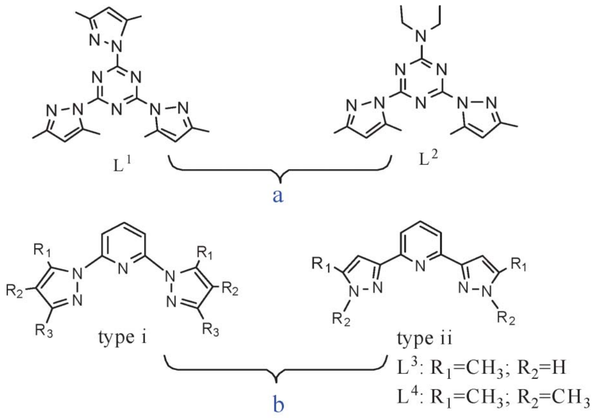

Scheme 1

In this paper, we successfully synthesized five novel different oxidation state vanadium(III, IV and V) complexes, $(VO)_2$(bpz*T-O) (**1**), VO(bpz*eaT)$(SCN)_2$ (**2**), V_2(bpz*eaT)$_2$(μ_2-C_2O_4)$(C_2O_4)_2$ (**3**), [VO(SO_4)(bpz*P)(H_2O)]·H_2O (**4**) and VO(SO_4)(bpz*P-Me)(H_2O) (**5**), with pincer *N*-heterocycle ligands for the first time and defined their structures by the X-ray crystallography method. In particular, the five complexes were tested for their bromination catalytic activity and the results indicate that they can be considered as a potential functional model of bromoperoxidase (V-BrPO).

Experimental section

All the chemicals used were of analytical grade and used without further purification. L^1 (tpz*T), L^2 (bpz*eaT),[27,28] L^3 (bpz*P-H) and L^4 (bpz*P-Me) were synthesized according to the modified literature method.[26b,29,30] Elemental analyses for C, H and N were carried out on a Perkin Elmer 240C automatic analyzer. Infrared spectra were recorded on a JASCO FT/IR-480 spectrometer with pressed KBr pellets in the range of 200–4000 cm^{-1}. UV-vis spectra were recorded on a JASCO V-570 spectrometer (200–2500 nm, in the form of a solid sample). Thermogravimetric analyses (TG) were performed under atmosphere with a heating rate of 10 °C min^{-1} on a Perkin Elmer Diamond TG/DTA.

$(VO)_2$(bpz*T-O) (1)

$VO(acac)_2$ (0.5 mmol, 0.082 g) and L^1 (0.5 mmol, 0.182 g) were dissolved in CH_3OH (10 mL), instantaneously giving a green solution which was stirred at room temperature for 4 h. Then, the solution was left at room temperature for a few days and yellow crystals were obtained in *ca.* 65% yield based on V(IV). Anal. calc. for $C_{13}H_{14}O_3N_7V$: C, 42.48; H, 3.81; N, 26.68. Found: C, 42.46; H, 3.84; N, 26.65%. IR (KBr, ν, cm^{-1}): 3439, ν(O–H); 2994, 2929, ν(C–H); 1637, ν(C=N) or ν(C=C); 1427, 770, δ(C–H); 958, ν(V=O); 444, ν(V–N). UV-vis (λ max, nm): 208, 280, π–π^*; 340, LMCT.

VO(bpz*eaT)$(SCN)_2$ (2)

$VOSO_4$ (0.5 mmol, 0.082 g), L^2 (0.5 mmol, 0.17 g) and KSCN (0.5 mmol, 0.041 g) were dissolved in CH_3CN (10 mL) with refluxing for 3 h at a temperature of 80 °C to get a blue solution. After filtration, the precipitate was dissolved in CH_2Cl_2. After two days, blue crystals suitable for X-ray diffraction were obtained in *ca.* 64.86% yield based on V(IV). Anal. calc. for $C_{19}H_{26}N_{10}OS_2V$: C, 43.38; H, 4.95; N, 26.64. Found: C, 43.43; H, 4.89; N, 26.60%. IR (KBr, ν, cm^{-1}): 3433, ν(O–H); 2978, 2932, ν(C–H); 2071, ν(SCN); 1649, ν(C=N) or ν(C=C); 1477, 766, δ(C–H); 964, ν(V=O); 448, ν(V–N). UV-vis (λ max, nm): 262, π–π^*; 350, LMCT; 768, d–d.

V_2(bpz*eaT)$_2$(μ_2-C_2O_4)$(C_2O_4)_2$ (3)

$V_2(SO_4)_3$ (0.5 mmol, 0.195 g), L^2 (0.5 mmol, 0.17 g) and $H_2C_2O_4$ (2.00 mmol, 0.18 g) were mixed and stirred for 2 h in a solution of H_2O and CH_3OH (12 mL, 2 : 1). Then, the mixture was sealed into a bomb and heated at 100 °C for 3 days, cooled to room temperature and brown crystals of **3** were obtained in *ca.* 27% yield (based on V(III)). Anal. calc. for $C_{40}H_{52}O_{14}N_{16}V_2$: C, 44.33; H, 4.80; N, 20.69. Found: C, 44.38; H, 4.92; N, 20.61%. IR (KBr, ν, cm^{-1}): 3421, ν(O–H); 2982, ν(C–H); 1712, 1696, $\nu_{as}(COO^-)$; 1399, $\nu_s(COO^-)$; 1652, ν(C=N) or ν(C=C); 1483, 792, δ(C–H); 469, ν(V–N). UV-vis (λ max, nm): 262, π–π^*; 316, 382, LMCT; 526, 676, d–d.

[VO(SO_4)(bpz*P)(H_2O)]·H_2O (4)

$V_2(SO_4)_3$ (0.25 mmol, 0.0975 g), L^3 (0.25 mmol, 0.0593 g), H_2O (10 mL) and EtOH (2 mL) were mixed in a 25 mL glass beaker. After stirring for 3 h, the mixture was sealed in a Teflon-lined autoclave and heated at 160 °C for three days, followed by slowly cooling to room temperature. After filtration, the filtrate was left at room temperature for several days until blue crystals suitable for X-ray diffraction were obtained in *ca.* 80.37% yield (based on V(III)). Anal. calc. for $C_{13}H_{17}O_7N_5SV$: C, 35.59; H, 3.89; N, 15.97. Found: C, 35.62; H, 3.92; N, 15.78%. IR (KBr, ν, cm^{-1}): 3609, 3487, ν(O–H); 3135, ν(N–H); 3074, ν(Ar–H); 2955, 2925, ν(C–H); 1617, 1553, 1445, 1270, 1024, ν(C=N), ν(C=C) or δ(C–C); 989, ν(V=O); 1148, ν(S–O); 585, δ(S–O). UV-vis (λ max, nm): 264, π–π^*; 322, LMCT; 582, 706, d–d.

VO(SO_4)(bpz*P-Me)(H_2O) (5)

The synthesis of **5** is similar to that of **4** but L^3 was replaced by L^4 (0.25 mL, 0.0668 g). Green crystals of **5** were obtained in *ca.* 80.37% yield (based on V(III)). Anal. calc. for $C_{15}H_{19}O_6N_5SV$: C, 40.15; H, 4.24; N, 15.61. Found: C, 40.19; H, 4.15; N, 15.70%. IR (KBr, ν, cm^{-1}): 3422, 3329, ν(O–H); 3097, ν(Ar–H); 2926, 2857, ν(C–H); 1616, 1570, 1449, 1238, 1011, ν(C=N), ν(C=C) or δ(C–C); 976, ν(V=O); 1173, ν(S–O); 607, δ(S–O). UV-vis (λ max, nm): 260, π–π^*; 336, LMCT; 596, 764, d–d.

X-ray crystallographic determination

Suitable single crystals of the five complexes were mounted onto glass fibers for X-ray measurements. The reflection data were collected at room temperature on a Bruker AXS SMART APEX II CCD diffractometer with graphite monochromatized Mo–Kα radiation (λ = 0.71073 Å) and a ω scan mode. All the measured independent reflections ($I > 2\sigma(I)$) were used in the structural analyses and semi-empirical absorption corrections were applied using the SADABS program.[31] The structures were solved by the direct method using SHELXL-97.[32] All non-hydrogen atoms were refined anisotropically. The hydrogen atoms of the organic frameworks were fixed geometrically at calculated positions and refined using a riding model but the hydrogen atoms of the lattice water molecules in **3**, **4** and **5** were found in a difference Fourier map. The structure of **2** (R_{int} = 0.0609) is not of perfect quality as a result of the low theta diffraction angle (θ_{max} = 22.8°), probably due to the small crystal size or poor crystal quality. The crystallographic data and the structure refinements are given in Table 1. The drawings were made with Diamond 3.2.

Quantum chemical calculation

First-principles density-functional theory (DFT) calculations have been carried out using the DMOL3 module in Materials Studio.[33,34] Double numerical basis sets for all the atoms with effective core potentials (ECP)[35,36] were used for the optimization of the three complexes. The PBE version of the generalized gradient approximation (GGA)[37] was used for the electron exchange and correlation. The convergence criteria for the charge density of self-consistent iterations were set to 10^{-6}, which allows the binding energy to converge to 10^{-6} Ry.[38] The Brillouin zone was sampled by 2 × 2 × 2 k-points using the Monkhorst–Pack scheme. The charge distribution on the system was analysed by the Mulliken method.[39] Based on the optimized structures obtained above, we calculated their energy levels and plotted the electron densities of the highest occupied molecular orbital (HOMO) and the lowest unoccupied molecular orbital (LUMO) at the Gamma point.

Measurement of the bromination activity in solution

Bromination reaction activity tests were carried out in a mixed solution of H_2O–DMF at a constant temperature of 30 $\pm$ 0.5 °C. The oxidovanadium complexes were dissolved by the addition of 25 mL of H_2O–DMF in the volume ratio of 4 : 1. The solutions used for the kinetic measurements were maintained at a constant concentration of H^+ (pH 5.8) by the addition a buffer solution of NaH_2PO_4–Na_2HPO_4.[40] The reactions were initiated by the addition of a phenol red solution. The oxidovanadium complexes with five different concentrations were placed in five different cuvettes and then the cuvettes were placed in a constant temperature water bath for 10 minutes and the spectral changes were recorded using a 721 UV-vis spectrophotometer at 5 min intervals. Finally, the resulting data were collected during the reaction and fitted

Table 1 Crystallographic data for complexes **1–5**

Complexes	**1**	**2**	**3**	**4**	**5**
Formula	$C_{13}H_{14}O_3N_7V$	$C_{19}H_{26}N_{10}OS_2V$	$C_{40}H_{52}O_{14}N_{16}V_2$	$C_{13}H_{17}O_7N_5SV$	$C_{15}H_{19}O_6N_5SV$
M (g mol^{-1})	367.25	523.54	1082.86	438.32	448.35
Temperature (K)	293(2)	293(2)	293(2)	293(2)	296(2)
Crystal system	Monoclinic	Monoclinic	Triclinic	Monoclinic	Monoclinic
Space group	$P2_1/n$	$P2_1/n$	$P\bar{1}$	$P2_1/n$	$P2_1/n$
a (Å)	9.378(2)	13.447(3)	9.3562(10)	8.0090(17)	12.260(2)
b (Å)	12.245(3)	8.7943(18)	11.9681(12)	12.111(3)	8.0264(15)
c (Å)	13.488(3)	22.021(4)	11.9868(12)	18.060(4)	19.192(4)
α (°)	90	90	60.215(2)	90	90
β (°)	92.744(3)	105.599(3)	84.303(2)	92.664(3)	102.580(2)
γ (°)	90	90	81.998(2)	90	90
V (Å^3)	1547.1(6)	410.85(14)	1152.9(2)	1749.8(6)	1843.3(6)
Z	4	1	1	4	4
D_{calc}	1.594	1.386	1.560	1.664	1.616
Crystal size (mm)	0.30 × 0.23 × 0.20	0.46 × 0.09 × 0.08	0.48 × 0.26 × 0.14	0.30 × 0.18 × 0.09	0.28 × 0.13 × 0.11
F(000)	768	1084	562	900	924
μ(Mo–Kα)/mm^{-1}	0.671	0.594	0.491	0.736	0.696
θ (°)	2.25–25.00	1.92–22.80	1.96–28.21	2.03–27.90	2.45–25.00
Reflections collected	7548	9995	5645	10 503	8938
Independent reflections($i > 2\sigma(i)$)	2726(2369)	3408(2206)	4010(3062)	4108(2599)	3239(2649)
R_{int}	0.0189	0.0609	0.0199	0.0518	0.0286
Parameters	217	298	329	244	253
$\Delta\rho$ (e Å^{-3})	0.526, −0.636	0.440, −0.400	0.519, −0.461	0.549, −0.612	0.500, −0.384
Goodness of fit	1.077	1.023	1.014	1.003	1.087
R^a	0.0455(0.1367)^b	0.0538(0.1201)^b	0.0507(0.1240)^b	0.0531(0.0927)^b	0.0443(0.0565)^b
$wR_2{}^a$	0.0519(0.1421)^b	0.0946(0.1401)^b	0.0737(0.1332)^b, (0.0674)^b	0.1334(0.1566)^b	0.1194(0.1263)^b

[a] $R = \Sigma||F_o| - |F_c||/\Sigma|F_o|$, $wR_2 = (\Sigma(w(F_o{}^2 - F_c{}^2)^2/\Sigma(w(F_o{}^2)^2)^{1/2}$; $[F_o > 4\sigma(F_o)]$. [b] Based on all the data.

using the curve-fitting software in the Microsoft Excel program.

It is assumed that the rate of this reaction is described by the rate equation: $dc/dt = kc_1{}^xc_2{}^yc_3{}^z$, from which the equation "$\log(dc/dt) = \log k + x \log c_1 + y \log c_2 + z \log c_3$" was obtained, corresponding to "$-\log(dc/dt) = -x \log c_1 - b$ ($b = \log k + y \log c_2 + z \log c_3$)", where k is the reaction rate constant; c_1, c_2, c_3 are the concentrations of the complex, KBr and phenol red, respectively, while x, y, z are the corresponding reaction orders. According to Lambert–Beer's law, $A = \varepsilon dc$, which as a differential is $dA/dt = \varepsilon d(dc/dt)$, where A is the measurable absorbance of the resultant; ε is the molar absorption coefficient, which for bromophenol blue is measured as 14 500 M^{-1} cm^{-1} at 592 nm; d is the light path length of the sample cell ($d = 1$). When the measurable absorbance data were plotted *versus* the reaction time, a line was obtained and the reaction rate of the complexes (dA/dt) was given by the slope of this line. By changing the concentration of the oxovanadium complexes in the reaction system, a series of dA/dt data can be obtained. The reaction rate constant (k) can be obtained according to a plot of $-\log(dc/dt)$ *versus* $-\log c_1$ and was fitted using the curve-fitting software in the Microsoft Excel program by generating a least squares fit to a general equation of the form "$y = mx - b$", in which "m" is the reaction order of the oxovanadium complexes in this reaction and "b" is the intercept of the line. In the experiment, considering that the reaction orders of KBr and phenol red (y and z) are 1 according to the literature,[32] c_2 and c_3 are known as 0.4 and 10^{-4} mol L^{-1}, respectively. Based on the equation "$b = \log k + y \log c_2 + z \log c_3$", the reaction rate constant (k) can be obtained. The bromination of phenol red was monitored by the measurement of the absorbance at 592 nm for reaction aliquots which were extracted at specific time points and diluted into a pH 5.8 phosphate buffer.

Results and discussion

Synthesis

We have successfully synthesized complexes **1–5** with a hydrothermal reaction for **3**, **4** and **5**, a solution reaction for **1** and a refluxing reaction for **2** (Scheme 2a). To meet the coordination conditions of the corresponding ligands and vanadium atom together in the reaction system, herein, we have endeavored to search for the most optimal reaction conditions. Hereinto, complex **1** was synthesized from the starting material VO(acac)$_2$(IV), while the experimental results indicate that the oxidation state of the vanadium atom of **1** is +5, which is confirmed by bond-valence theory.[41,42] This is because an unsaturated ketone conjugate structure in complex **1** is formed by an *in situ* reaction of one 3,5-dimethylpyrazolyl group in the 2-position of the L^1 ligand,[43] the central vanadium metal being oxidized *via* [O] during the reaction (Scheme 2b). Its lower density cloud electron draws the d-electrons of the vanadium(IV) atom, which leads to a change in the valence of the central metal atom (from +4 to +5). We initially used a solution method to synthesize complex **2**, however, we could not obtain the corresponding complex. Then we attempted to use a refluxing method with CH_3CN and

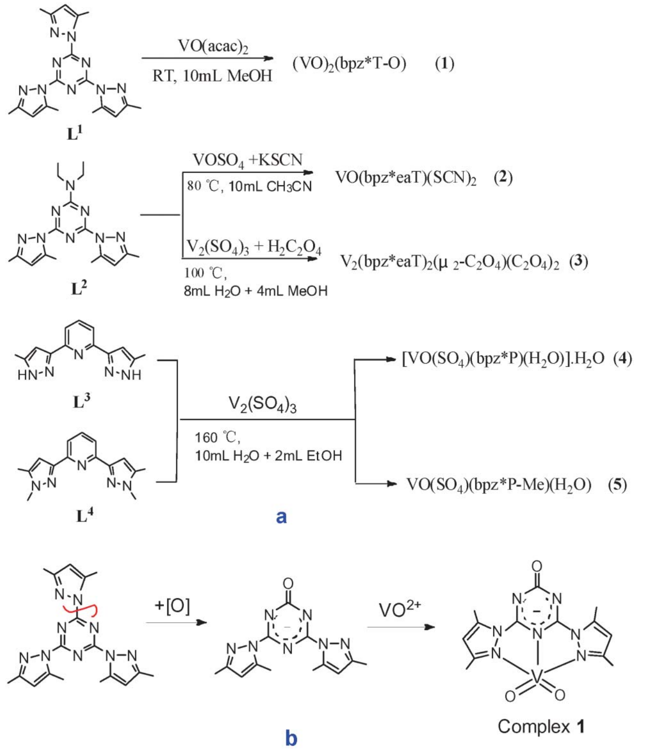

Scheme 2 a: The synthetic routes of complexes **1–5**; b: the detail reaction mechanism routes of complex **1**.

only got the powder of **2**, which was recrystallized in CH_2Cl_2 to get nice single crystals. The synthesis of complex **3** was subject to experimentation in a mixed system of water and methanol at temperatures of 120 °C, 140 °C and 160 °C. Unfortunately, it failed so we readjusted the temperature at 100 °C and successfully got single crystals of the corresponding complex **3**. According to the experiences of previous experiments,[44] we successfully obtained complexes **4** and **5** in a mixed solution system of ethanol and water (1 : 5).

It is interesting to note that starting materials of V(III) were used in the synthesis process of complexes **3**, **4** and **5**. However, the valence of the central metal of **4** and **5** has been changed. A possible reason is that the higher temperature could lead to V(III) atom being oxidized into a V(IV) or V(V) atom by the oxygen in air.

Crystal structure analysis

The molecular structures of complexes **1–5** are depicted in Fig. 1–5, respectively. The principal bond distances and angles for complexes **1–5** are summarized in Table 2. The relevant H-bond parameters of complexes **1–5** are listed in Table 3. The deviations of the coordinated atoms out of the equatorial plane for **1–5** are listed in Table S1, ESI.†

Structure of complex 1. Complex **1** was synthesized with the L^1 ligand to link one vanadium atom and adopt a pincer tridentate coordination mode. This vanadium atom is coordinated by two terminal oxygen atoms (O2, O3) and three nitrogen atoms (N1, N5 and N6) from the L^1 ligand, with N1, O2 and O3 located in the equatorial plane and N5 and N6 stood in the axial positions (Fig. 1a). The structure of **1** can be evaluated by the Addision distortion index τ:[45,46] $\tau = (\beta - \alpha)/60°$, where β and α are the largest angles ($\beta > \alpha$) around a five-coordinate metal center. In a pentacoordinated system, the values for τ in an ideal polyhedra are 1.0 for a trigonal bipyramid and 0.0 for a square pyramid. The value of τ for the metal center of complex **1** is 0.60, indicating that the coordination environment of the vanadium atom is close to distorted trigonal bipyramidal. The deviations of the N1, O2 and O3 atoms that comprise the least-squares plane are all 0.0000 Å, showing that these atoms are on one plane. The V, N5 and N6 from the axial position lie −0.0088, 1.9807 and −1.9961 Å out of the equatorial plane, indicating that the V atom is located in the middle of the N5 and N6 atoms. Furthermore, the pyrazolyl rings from two sides are distorted to the least-squares plane (central triazine ring), with the dihedral angle varying from 1.3(4) to 1.8(4)°. The bond lengths of V–N and V–O are in the range of 2.060(3)–2.085(3) Å and 1.604(2)–1.609(2) Å, respectively. The O–V–O, O–V–N and N–V–N angles are in the range of 109.65(13)°, 99.36(12)–128.08(12)° and 72.55(10)–145.37(10)°, respectively.

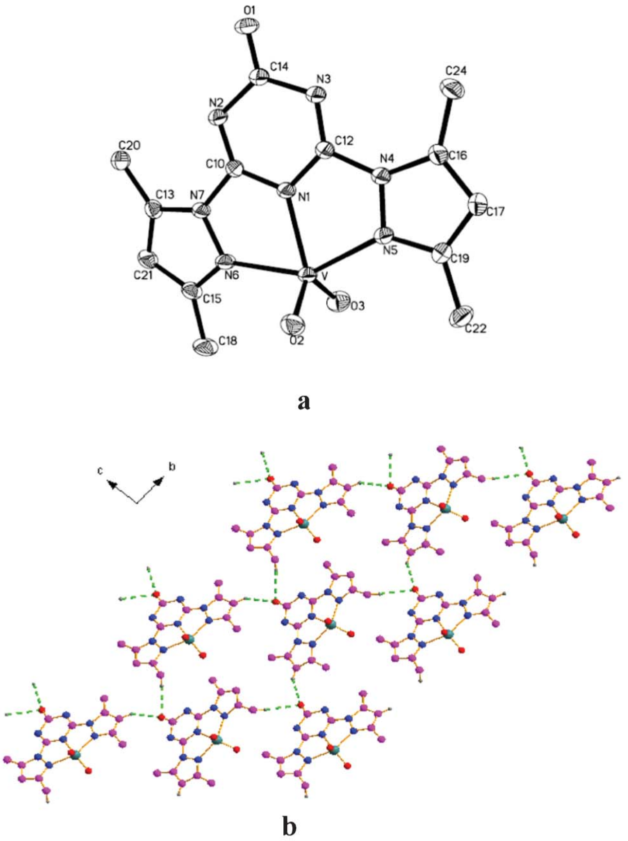

Fig. 1 (a): The molecular structure of **1**; (b): a view of the two-dimensional hydrogen bonding network in **1**. (All H atoms expect for the hydrogen bonds are omitted for clarity.)

In addition, in the molecule of complex **1**, there are important C–H···O hydrogen bonds (3.3184, 3.3874 Å), as illustrated in Fig. 1b. The hydrogen bonds come from between the pyrazolyl ring ($C21^{\#1}$ and $C22^{\#1}$, #1: $-0.5 + x$, $0.5 - y$, $0.5 +$

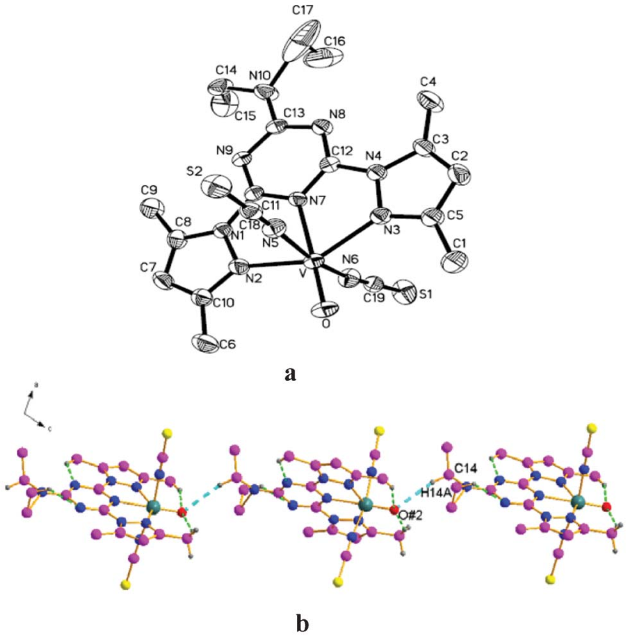

Fig. 2 (a): The molecular structure of **2**; (b): a fragment of the 1D chain with hydrogen bonding interactions along the *b*-axis in **2**. (All H atoms expect for the hydrogen bonds are omitted for clarity.)

z) and the unsaturated ketone group of the triazine ring (O1). Independent molecules are linked to form a 2D sheet structure *via* the two types of hydrogen bonds.

Structure of complex 2. The asymmetric unit of **2** is completed by one vanadium atom, one coordinated L^2 ligand and two –SCN groups and the coordination mode of the L^2 ligand is similar to that of **1**, acting as a pincer tridentate coordination mode. The environment around the V atom can be described as a distorted octahedral geometry and it is coordinated by one terminal oxygen (O), two nitrogen atoms (N5, N6) from two –SCN groups and three nitrogen atoms (N2, N3 and N7) from the L^2 ligand (Fig. 2a). The deviations of the N2, N3, N5 and N6 atoms that comprise the least-squares plane are −0.2226, −0.2321, 0.2260 and 0.2287 Å, respectively, showing that these atoms are close on one plane. The V, N7 and O from the axial position lie 0.4435, −1.7060 and 2.0320 Å out of the equatorial plane, indicating that V is towards the O and *trans* to N7. The bond distances of $V–N_{SCN}$ and $V–N_{L}{}^2$ are in the range of 2.027(5)–2.039(5) Å and 2.120(4)–2.150(4) Å, respectively. The N–V–N bond angles are in the range of 71.54(15) to 167.62(17)°. Furthermore, the pyrazolyl rings from two sides are distorted to the least-squares plane (central triazine ring) with the dihedral angle varying from 3.2(3) to 3.0(3)°. The V–N bond length is in the range of 2.027(5)–2.150(4) Å and the V–O bond length is 1.589(3) Å, respectively. The O–V–N and N–V–N angles are in the range of 95.62(17)–178.56(18)° and 71.54(15)–167.62(17)°, respectively.

There are abundant intra- and inter-hydrogen bonds in the structure, such as C1–H1A⋯O (3.4143 Å), C6–H6A⋯O (3.3470 Å), C9–H9A⋯N9 (2.9666 Å), C14–H14A⋯O (3.4772 Å) and C16–H16C⋯N8 (2.9836 Å) in complex **2**, as illustrated in Fig. 2b. Here, the inter-hydrogen bond of C14–H14A⋯O[#2] (#2: −0.5 + *x*, 0.5 − *y*, −0.5 + *z*) comes from the carbon in the dimethylamino group of the L^2 ligand and the terminal oxygen, which forma a 1D chain. In the mean time, the other intra-hydrogen bonding interactions could make the structure of complex **2** more stable.

Structure of complex 3. The asymmetric unit of complex **3** consists of two V atoms, two L^2 ligands and three oxalic acid ligands. The coordination environment of the vanadium atom is shown in Fig. 3a. V(III) is seven-coordinate with three N atoms (N1, N5 and N7) from the L^2 ligand with V–N bond lengths in the range of 2.129(3)–2.259(3) Å, four oxygen atoms (O1, O2, O3 and O4) from the oxalic acid ligands, hereinto, O1 and O2 come from a bridging oxalic acid with $V–O_{bridging}$ bond lengths in the range of 2.094(2)–2.127(2) Å, and O3 and O4 are from a terminal oxalic acid with $V–O_{terminal}$ bond lengths in the range of 1.990(2)–1.996(2) Å, to form a distorted pentagonal bipyramidal geometry. The molecular structure is centrosymmetric and the centre of inversion is located on the C–C bond of the bridging oxalate moiety with a V⋯V contact of 5.5024(11) Å. The deviations of the O1, O3, N1, N5 and N7 atoms that comprise the least-squares plane are 0.5165, −0.2415, 0.4646, −0.6358 and −0.1038 Å, respectively, showing that these atoms are close on one plane. The V1, O2 and O4 atoms from the axial position lie −0.0878, 1.9732 and −2.0678 Å out of the equatorial plane. Furthermore, the pyrazolyl rings from two sides are distorted to the least-squares plane (central triazine ring) with the dihedral angle varying from 10.1(2) to 11.9(2)°. The O–V–O, O–V–N and N–V–

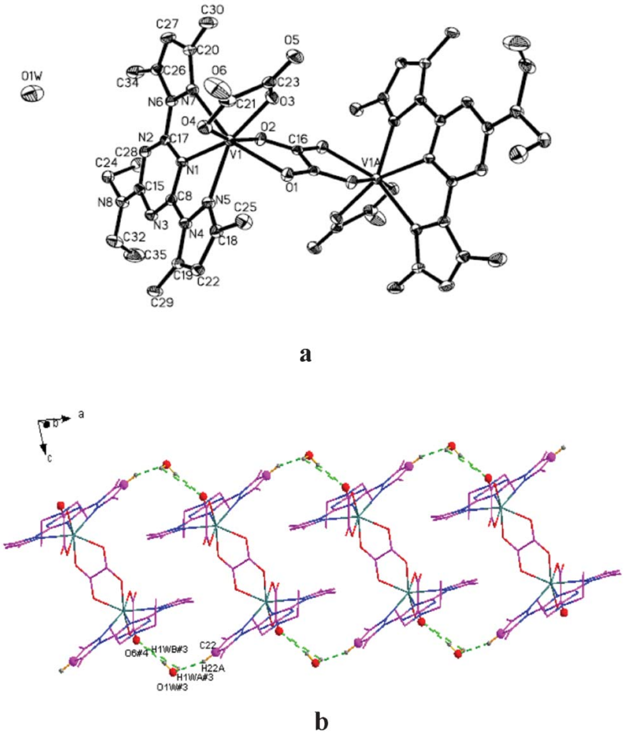

Fig. 3 (a): The molecular structure of **3**; (b): a view of the 1D chain from the hydrogen bonding interactions in **3**. (All H atoms expect for the hydrogen bonds are omitted for clarity.)

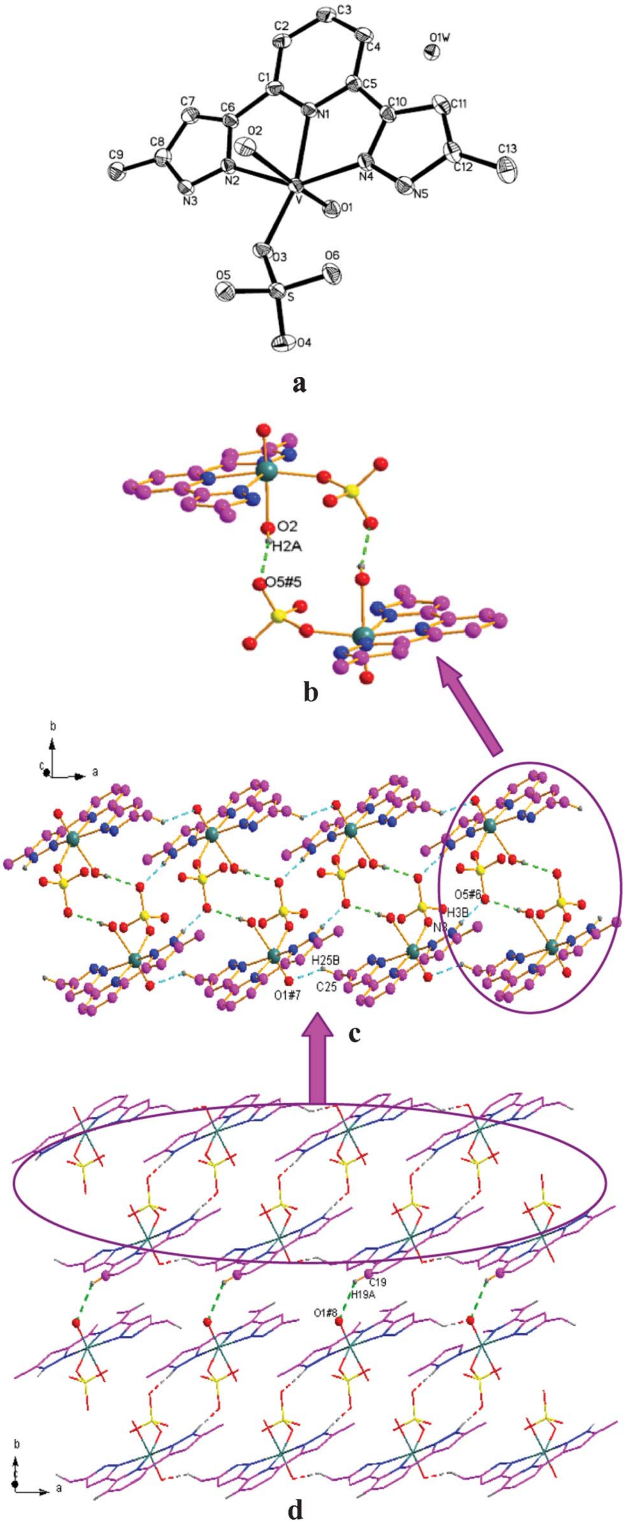

Fig. 4 (a): The molecular structure of **4**; (b): the dimer from the hydrogen bonding interactions; (c): a view of the 1D chain from the hydrogen bonding interactions in **4**. (d): A view of the two-dimensional hydrogen bonding network. (All H atoms expect for the hydrogen bonds are omitted for clarity.)

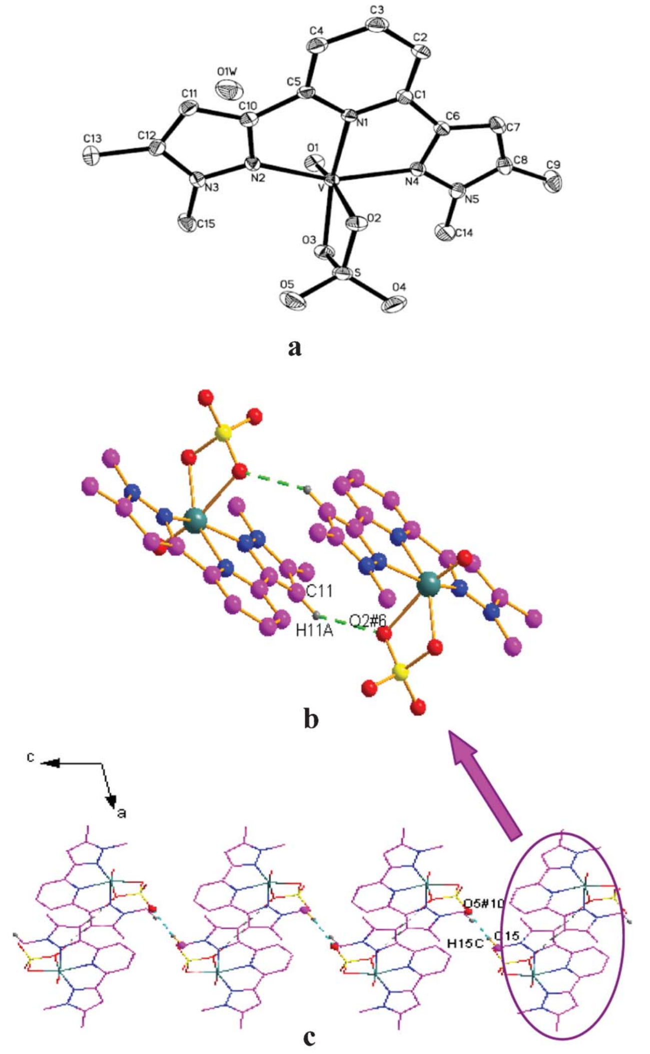

Fig. 5 (a): The molecular structure of **5**; (b): the dimer from the hydrogen bonding interactions; (c): a view of the 1D chain from the hydrogen bonding interactions in **5**. (All H atoms except for the hydrogen bonds are omitted for clarity.)

N angles are in the range of 77.34(10)–165.19(10)°, 73.22(10)–152.20(11)° and 69.20(10)–130.47(10)°, respectively.

In addition, in the molecular structure, there are three kinds of hydrogen bonds: (i) hydrogen bond (O–H⋯O: O1W$^{\#3}$–H1WA$^{\#3}$⋯O6$^{\#4}$ and O1W$^{\#3}$–H1WB$^{\#3}$⋯O6$^{\#4}$, #3: $-x$, $1 - y$, $1 - z$. #4: $-1 + x$, y, z) between the oxygen from the lattice water and the carboxylate oxygen from the oxalic acids; (ii) hydrogen bond (C–H⋯O: C22–H22A⋯O1W$^{\#3}$ and C30–H30A⋯O3) between the carbon atoms from the L^2 ligand and the oxygen atoms from the lattice water and oxalic acid molecules; (iii) hydrogen bond (C–H⋯N: C29–H29A⋯N3) between the carbon and the nitrogen atoms from the L^2 ligand. Through the hydrogen bonds of C22–H22A⋯O1W$^{\#3}$, O1W$^{\#3}$–H1WA$^{\#3}$⋯O6$^{\#4}$ and O1W$^{\#3}$–H1WB$^{\#3}$⋯O6$^{\#4}$, the molecules of the complex **3** are connected into an infinite 1D chain structure (Fig. 3b) and the lattice water is very important to link the vanadium complex moiety *via* these hydrogen bonding interactions.

Table 2 Crystallographic data for complexes **1–5**

Complex **1**			
V–O2	1.604(2)	N1–V–N5	72.55(10)
V–O3	1.609(2)	O2–V–N6	101.04(11)
V–N1	2.060(3)	O3–V–N6	99.36(12)
V–N5	2.081(3)	N1–V–N6	72.92(10)
V–N6	2.085(3)	N5–V–N6	145.37(10)
O2–V–O3	109.65(13)	O2–V–N5	99.38(11)
O2–V–N1	122.26(12)	O3–V–N5	99.69(12)
O3–V–N1	128.08(12)		
Complex **2**			
V–O	1.589(3)	O–V–N2	107.48(17)
V–N6	2.027(5)	N6–V–N2	89.19(17)
V–N5	2.039(5)	N5–V–N2	88.95(17)
V–N3	2.120(4)	N3–V–N2	143.16(15)
V–N2	2.127(4)	O–V–N7	178.56(18)
V–N7	2.150(4)	N6–V–N7	84.54(16)
O–V–N6	96.61(18)	N5–V–N7	83.26(15)
O–V–N5	95.62(17)	N3–V–N7	71.54(15)
N6–V–N5	167.62(17)	N2–V–N7	71.63(15)
O–V–N3	109.36(17)	N6–V–N3	86.67(16)
N5–V–N3	87.49(16)		
Complex **3**			
V–O4	1.990(2)	O2–V–O1	77.44(9)
V–O3	1.996(2)	O4–V–N1	110.30(11)
V–O2	2.094(2)	O3–V–N1	152.20(11)
V–O1	2.127(2)	O2–V–N1	79.81(10)
V–N1	2.129(3)	O1–V–N1	122.03(10)
V–N5	2.229(3)	O4–V–N5	79.96(10)
V–N7	2.259(3)	O3–V–N5	138.58(11)
O4–V–O3	79.97(10)	O2–V–N5	114.34(10)
O4–V–O2	165.19(10)	O1–V–N5	73.22(10)
O3–V–O2	86.26(10)	N1–V–N5	69.20(10)
O4–V–O1	104.53(10)	O4–V–N7	89.62(11)
O3–V–O1	77.34(10)	O3–V–N7	85.10(10)
N5–V–N7	130.47(10)	O2–V–N7	83.76(10)
N1–V–N7	69.64(10)	O1–V–N7	154.94(10)
Complex **4**			
V–O1	1.593(3)	N1–V–N2	76.13(11)
V–O3	1.968(2)	O1–V–N4	95.82(13)
V–N1	2.085(3)	O3–V–N4	108.75(11)
V–N2	2.110(3)	N1–V–N4	74.65(12)
V–N4	2.110(3)	N2–V–N4	148.97(12)
V–O2	2.223(3)	O1–V–O2	176.86(12)
O1–V–O3	99.26(13)	O3–V–O2	83.39(11)
O1–V–N1	97.15(12)	N1–V–O2	80.37(11)
O3–V–N1	162.76(11)	N2–V–O2	83.36(11)
O1–V–N2	97.95(13)	N4–V–O2	81.70(11)
O3–V–N2	96.30(11)		
Complex **5**			
V–O1	1.592(2)	N1–V–N2	75.65(10)
V–O3	2.001(2)	O1–V–N4	97.08(12)
V–N1	2.074(3)	O3–V–N4	102.51(10)
V–N2	2.100(3)	N1–V–N4	75.56(10)
V–N4	2.101(3)	N2–V–N4	150.62(10)
V–O2	2.228(2)	O1–V–O2	167.86(11)
O1–V–O3	101.45(12)	O3–V–O2	66.45(9)
O1–V–N1	107.45(12)	N1–V–O2	84.67(9)
O3–V–N1	151.06(10)	N2–V–O2	86.53(10)
O1–V–N2	96.99(12)	N4–V–O2	85.08(10)
O3–V–N2	99.79(10)		

Table 3 Hydrogen bonds (Å) of complexes **1–5**

D–H···A	*d*(D–H)/Å	*d*(H···A)/Å	*d*(D···A)/Å	∠D–H···A/°
Complex **1**				
C22$^{\#1}$–H22C$^{\#1}$···O1	0.9600	2.5516	3.3874	145.60
C21$^{\#1}$–H21A$^{\#1}$···O1	0.9300	2.5494	3.3184	140.28
Complex **2**				
C1–H1A···O	0.9600	2.5479	3.4143	150.16
C6–H6A···O	0.9600	2.4775	3.3470	150.57
C9–H9A···N9	0.9600	2.2155	2.9666	134.30
C14–H14A···O$^{\#2}$	0.9700	2.5223	3.4772	168.08
C16–H16C···N8	0.9600	2.2700	2.9836	130.44
Complex **3**				
O1W$^{\#3}$–H1WA$^{\#3}$···O6$^{\#4}$	0.8500	2.1572	2.9459	154.23
O1W$^{\#3}$–H1WB$^{\#3}$···O6$^{\#4}$	0.7781	2.3757	3.1134	158.67
C22–H22A···O1W$^{\#3}$	0.9600	2.5210	3.3833	149.47
C29–H29A···N3	0.9600	2.2300	2.9703	133.15
C30–H30A···O3	0.9600	2.4245	3.1494	132.07
Complex **4**				
O1w–H1wA···O3	0.8500	2.4745	3.1792	140.84
O2–H2A···O5$^{\#5}$	0.8500	2.1179	2.9313	160.04
N3–H3B···O5$^{\#6}$	0.8600	1.9579	2.8028	167.13
N5–H5A···O6	0.8600	2.0342	2.7222	136.38
C17–H17A···O1w	0.9300	2.5853	3.3186	136.09
C19–H19A···O1$^{\#8}$	0.9300	2.5613	3.3018	136.88
C22–H22A···O6$^{\#9}$	0.9300	2.3713	3.2586	159.46
C25–H25B···O1$^{\#7}$	0.9600	2.5099	3.2741	136.54
Complex **5**				
O1w–H1wB···O2	0.8500	2.3527	2.9156	124.11
C11–H11A···O2$^{\#6}$	0.9300	2.4901	3.2869	143.82
C15–H15A···O3	0.9600	2.4900	3.3649	151.50
C15–H15C···O5$^{\#10}$	0.9600	2.5045	3.2003	131.79

#1: $-0.5 + x, 0.5 - y, 0.5 + z$; #2: $-0.5 + x, 0.5 - y, -0.5 + z$; #3: $-x, 1 - y, 1 - z$; #4: $-1 + x, y, z$; #5: $-x, 2 - y, -z$; #6: $1 - x, 2 - y, -z$; #7: $-1 + x, y, z$; #8: $-x, 1 - y, -z$; #9: $0.5 + x, 1.5 - y, 0.5 + z$; #10: $1 - x, -0.5 + y, 0.5 - z$.

Structures of complexes 4 and 5. Single-crystal X-ray structure analyses revealed that each vanadium atom of the two complexes shows a distorted octahedral geometry defined by the N_3O_3 donor set. For complex **4**, the vanadium atom is coordinated by a terminal oxygen (O1), one oxygen atom (O2) from the coordinated water, one oxygen atom (O3) from the sulfate group and three nitrogen atoms (N1, N2, N4) from the L^3 ligand (Fig. 4a), forming a slightly distorted octahedral vanadium center, with N1, N2, N4 and O3 in the equatorial plane and O1 and O2 in the axial positions. The deviations of the N1, N2, N4 and O3 atoms that comprise the least-squares plane are 0.0164, −0.0139, −0.0130 and 0.0105 Å, respectively, showing that these atoms are almost on one plane. The V, O1 and O2 atoms from the axial position lie −0.2738, −1.8658 and 1.9485 Å out of the equatorial plane. The O1–V–O2 angle for complex **4** is 176.86(12)°. The L^3 ligand adopts a pincer tridentate chelate mode to coordinate with vanadium. For the sulfate group anion, one oxygen atom is coordinated to the vanadium with a monodentate coordination mode and moreover, the distance of the coordinated S–O (1.509(2) Å) is slight longer than the uncoordinated S–O (1.436(3) Å, 1.438(3) Å, 1.450(3) Å). The V–O1 bond length is 1.593(3) Å, while the V–O2 and V–O3 distances are 2.224(3) and 1.968(2) Å, respectively, which indicates that V–O1 is a double bond and V–O2 and V–O3 are single bonds. Hereinto, it is found that the length of V–O2 is obviously longer than V–O3, which shows that the coordination ability of the sulfate group is stronger than water. Similarly, the pyrazolyl rings from two sides are distorted to the least-squares plane (central pyridyl ring), with the dihedral angle varying from 2.8(3) to 4.9(3)°.

There are three kinds of hydrogen bonds, O–H···O (2.9313–3.1792 Å), C–H···O (3.2586–3.3186 Å) and N–H···O (2.7222–2.8028 Å), in **4**. Hereinto, the O–H···O hydrogen bond comes from the lattice water molecules and coordinated sulfate groups: O1w–H1wA···O3 (3.1792 Å), and between the coordinated water molecules and uncoordinated sulfate groups: O2–H2A···O5$^{\#5}$ (2.9313 Å, #5: $-x$, $2 - y$, $-z$); the C–H···O hydrogen bonds are from the carbon atoms of the L^3 ligand, lattice water molecules, terminal oxygen atoms and uncoordinated sulfate groups: C17–H17A···O1w (3.3186 Å), C19–H19A···O1$^{\#8}$ (3.3018 Å, #8: $-x$, $1 - y$, $-z$), C22–H22A···O6$^{\#9}$ (3.2586 Å, #9: $0.5 + x$, $1.5 - y$, $0.5 + z$) and C25–H25B···O1$^{\#7}$ (3.2741 Å, #7: $-1 + x$, y, z); the N–H···O hydrogen bonds come from the uncoordinated N atoms of the L^3 ligand and the uncoordinated sulfate groups: N3–H3B···O5$^{\#6}$ (2.8028 Å, #6: $1 - x$, $2 - y$, $-z$) and N5–H5A···O6 (2.7222 Å). Two independent molecules form a dimer *via* a O2–H2A···O5$^{\#5}$ hydrogen bonding interaction (Fig. 4b). The dimer is further linked through the N3–H3B···O5$^{\#6}$ and C25–H25B···O1$^{\#7}$ hydrogen bonds to generate a 1D chain structure, as illustrated in Fig. 4c, and then the adjacent chains are connected through C19–H19A···O1$^{\#8}$ hydrogen bonds to form a 2D sheet structure (Fig. 4d). In addition, *via* the corresponding C22–H22A···O6$^{\#9}$ hydrogen bond, adjacent sheets form a 3D structure.

For **5**, the coordination environment of the central vanadium atom is similar to that of **4**. The vanadium atom is coordinated by a terminal oxygen (O1), two oxygen atoms (O2, O3) from the sulfate group and three nitrogen atoms (N1, N2, N4) from the L^4 ligand (Fig. 5a), forming a slightly distorted octahedral vanadium center, with N1, N2, N4 and O3 in the equatorial plane and O1 and O2 in the axial positions. The deviations of the N1, N2, N4 and O3 atoms that comprise the least-squares plane are 0.1662, −0.1367, −0.1343 and 0.1048 Å, respectively, showing that these atoms are almost on one plane. The V, O1 and O2 from the axial position lie −0.3733, −1.9640 and 1.8224 Å out of the equatorial plane. The O1–V–O2 angle for the complex is 167.86(11)°. The coordination mode of the L^4 ligand is the same as complex **4** but the coordination mode of the sulfate group shows a bidentate chelate mode, while a similar trend for the bond lengths of S–O was observed in complex **5**, namely, S–O (coordinated) > S–O (uncoordinated). In complex **5**, the length of V–O1 is 1.592(2) Å, while the distances of V–O2 and V–O3 are 2.001(2) and 2.228(2) Å, which indicates that V–O1 is a double bond and V–O2 and V–O3 are single bonds. Furthermore, the pyrazolyl rings from two sides are distorted to the least-squares plane (central pyridyl ring) with the dihedral angle varying from 7.7(2) to 6.6(2)°.

Similarly, there are also two kinds of hydrogen bonds: O–H···O and C–H···O, in **5**. The O–H···O hydrogen bond comes from the lattice water molecule and coordinated sulfate group: O1w–H1wB···O2 (2.9156 Å); the C–H···O hydrogen bond is from among the carbon atoms of the L^4 ligand, the coordinated sulfate groups and the uncoordinated sulfate groups: C11–H11A···O2$^{\#6}$ (3.2869 Å), C15–H15A···O3 (3.3649 Å) and C15–H15C···O5$^{\#10}$ (3.2003 Å, #10: $1 - x$, $-0.5 + y$, $0.5 - z$). Two independent molecules form a dimer *via* the hydrogen bonding interaction of C11–H11A···O2$^{\#6}$ (Fig. 5b) and the dimer is further linked through C15–H15C···O5$^{\#10}$ hydrogen bonds to generate a one-dimensional chain on the *b*-axis, as illustrated in Fig. 5c.

It is found that the bond lengths of V–N1, V–N2 and V–N4 of **4** are slightly longer than those of **5**, which could be due to the electron donor group of "–CH$_3$" increasing the electron cloud density of the center metal for **5**. The same reason results in the V–O2 distance of **5** being longer than the V–O3 distance of **4**. However, the bond length of V–O3 in **5** is longer than that in **4**, which attributed to the *trans* effect of the terminal oxygen atom in complex **5**.

Quantum chemistry calculations of complexes 1–5

According to molecular orbital theory, the frontier orbitals and nearby molecular orbitals are the most important factors for the stability. The larger the difference between the frontier orbitals, the more stable the molecular structure.[47–49] The frontier molecular orbital symmetry and eigenvalues in Hartrees for complexes **1–5** are listed in Table S2, ESI.† The highest occupied molecular orbitals (HOMO): −0.2625, −0.1819, −0.1850, −0.1829 and −0.1773 a.u; the lowest unoccupied molecular orbitals (LUMO): −0.1495, −0.1818, −0.1834, −0.1827 and −0.1769 a.u. The gap (eV) is 3.074, 0.002, 0.037, 0.005 and 0.009, respectively. This shows that the order of thermodynamic stability for the complexes is **1** > **3** > **5** > **4** > **2**. The atomic net charges for the complexes calculated at the PBE level are shown in Table S3, ESI.† The net charges of the central vanadium in complexes **1–5** are in the range of 0.422 to 1.113 eV, deviating from their +3, +4, +5 valences, respectively. This shows that the d orbit of the metal vanadium partly obtained electrons from the ligand (L^1, L^2, L^3 or L^4) and the sulfate group. The average net charges of the oxygen atom from the coordinated water (−0.608 eV for **4**) is a little more negative than those of the coordinated oxygen atoms from the sulfate ion (−0.541 eV for **4**, −0.569 eV for **5**) and more negative than that of the coordinated oxygen atoms from the oxalic acid ligands (−0.477 eV for **3**). The average net charges of the terminal oxygen atoms for **1–5** are −0.481, −0.471, −0.539, −0.571, −0.604 eV, respectively. In complexes **1–3**, the average net charges of the coordinated nitrogen atoms from the pyrazolyl rings are −0.198, −0.205 and −0.202 eV, respectively. In complexes **4** and **5**, the average net charges of the coordinated nitrogen atoms from the pyrazolyl rings are −0.302 and −0.209 eV, showing that the order of the average net charge of the nitrogen atoms in complexes **1–5** is: $N_{\text{pyrazolyl(triazine ring)}} > N_{\text{pyrazolyl(pyridine ring)}}$, which may be attributed to the larger degree of conjugation of the triazine ring.

Thermal properties

To examine the thermal stability of complexes **1–5**, thermogravimetric analysis (TG) was carried out at a heating rate of 10 °C min^{-1} under nitrogen in the temperature range of 30–1000 °C (Fig. 6). In **1**, the results show that the initial weight loss of 49.2% before 582 °C is due to the release of two 3,5-dimethyl pyrazolyl moieties (calc. 51.6%). The second weight loss occurs in the temperature range of 582–1000 °C, which is ascribed to

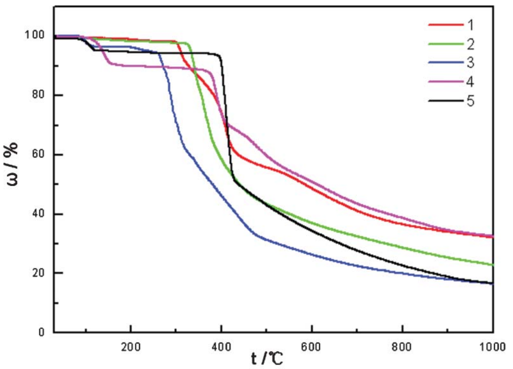

Fig. 6 TG curves of complexes **1–5**.

the release of the framework of the triazine ring of the L^1 ligand, and the final residue corresponds to vanadium oxide and nitride. In **2**, the first weight loss of 15.26% is attributed to the reduction of the diethylamine of the L^2 ligand (calc. 13.75%) in the temperature range of 323–352 °C. The second weight loss of 59.88% was attributed to the release of two –SCN groups and two 3,5-dimethyl pyrazolyl moieties (calc. 62.28%) in the temperature range of 352–1000 °C. The final residue corresponds to the vanadium atom and triazine ring (obsd: 22.83%; calc.: 24.64%). In **3**, the initial weight loss of 3.33% before 113 °C corresponds to the release of two lattice water molecules (calc. 3.32%). The second weight loss of 80.13% is attributed to the reduction of two L^2 ligands and two terminal oxalic acid molecules (calc. 79.42%) in the temperature range of 195–1000 °C, and the final residue corresponds to two vanadium atoms and oxalic acid molecules in the bridge site. In **4**, the results show an initial weight loss of 8.42% before 156 °C which is due to the release of a lattice water and a coordinated water molecule (calc. 8.21%). The second weight loss occurs in the temperature range of 156–1000 °C, which is ascribed to the release of the framework of the L^3 ligand and the sulfate iron. The thermal stability of complex **5** is similar to that of complex **4**. The first stage occurs in the temperature region of 40–120 °C, with a mass loss of 3.97% corresponding to the loss of one lattice water (calc. 4.01%). The last step is observed in 120–1000 °C, which is considered to be the gradual decomposition of the framework of the ligands. The residues correspond to the vanadium nitride compound for both **4** and **5**.

Functional mimic of vanadium haloperoxidase

Mimicking bromination reaction of the complexes. To our knowledge, oxidovanadium complexes are able of mimicking a reaction in which vanadium haloperoxidases catalyze the bromination of organic substrates in the presence of H_2O_2 and bromide. For example, the bromination of trimethoxybenzene,[50] benzene, salicylaldehyde and phenol is catalyzed by the VO_2^+ moiety,[51] and the bromination of phenol red by $[VO(O2)H_2O]^+$ and its related species.[52] Herein, the bromination reaction activities of **1–5** using phenol red as an organic substrate, which is shown by the conversion of phenol red to bromophenol blue, have been investigated. The reaction is rapid and stoichiometric, producing the halogenated product by the reaction of the oxidized halogen species with the organic substrate.

The addition of a solution of **1** to the standard reaction of bromide in a phosphate buffer with phenol red as a trap for the oxidized bromine resulted in a visible color change of the solution from yellow to blue. As shown in Fig. 7, a decrease in the absorbance of the peak at 443 nm due to the loss of phenol red and an increase in the absorbance of the peak at 592 nm characteristic of the bromophenol blue product is seen, showing that complex **1** possesses significant catalytic activities. The results of the mimicking catalytic activities for **2–5** are similar to that of **1**.

Kinetic studies of the mimicking bromination reaction. Taking complex **1** as an example, a series of dA/dt data was obtained (Fig. 8) by changing the concentration of the oxovanadium complex. (The measurable absorbance dependence on time for complexes **2–5** is shown in Fig. S1, ESI.†)

According to the data in Fig. 8, the plot of $-\log(dc/dt)$ *vs.* $-\log c$ for complex **1** is depicted and gave a straight line with a slope of 1.0527 and $b = -2.2581$, as shown in Fig. 9. The former confirmed that the reaction order is first-order reaction dependence on vanadium. Based on the equation "$b = \log k + y \log c_2 + z \log c_3$", the reaction rate constant, k, is determined by the concentrations of KBr and phenol red (c_2 and c_3), the reaction orders of KBr and phenol red (y and z) and b. In the experiment, considering that the reaction orders of KBr and phenol red (y and z) are 1 according to the literature,[53,54] c_2 and c_3 are known to be 0.4 mol L^{-1} and 10^{-4} mol L^{-1}, respectively, so the reaction rate constant (k) for **1** can be calculated as 0.14×10^3 (mol $L^{-1})^{-2}$ s^{-1} ($-\log(dc/dt)$ dependence of $-\log c$ for **2–5** is shown in Fig. S2, ESI†).

Similar plots for **2–5** were generated in the same way. The kinetic data for **2–5** in DMF–H_2O at 30 ± 0.5 °C are shown in Table 4. It is found that: (i) the reaction orders of the oxidovanadium complexes in the bromination reaction are all close to 1, confirming the first-order dependence on vanadium; (ii) the order of the reaction rate constants for them is **4** > **5** > **3** > **2** > **1**.

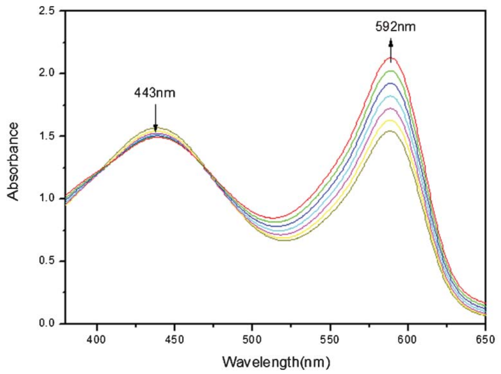

Fig. 7 Oxidative bromination of phenol red was catalyzed by **1**. Spectral changes at 10 min intervals. The reaction mixture contained a phosphate buffer (pH 5.8), KBr (0.4 mol L^{-1}), phenol red (10^{-4} mol L^{-1}) and complex **1** (0.1 μmol L^{-1}).

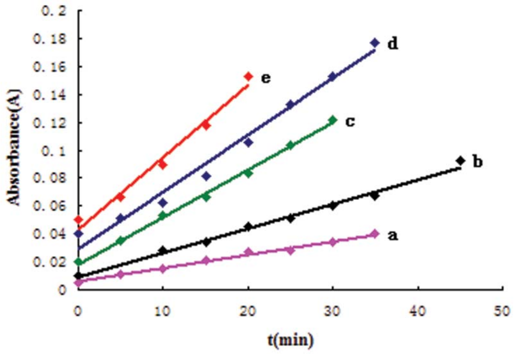

Fig. 8 The measurable absorbance dependence on time for complex **1**. Conditions used: pH = 5.8, c(KBr) = 0.4 mol L^{-1}, $c(H_2O_2)$ = 1 mmol L^{-1}, c(phenol red) = 10^{-4} mol L^{-1}. c(complex **1**/mmol L^{-1}) = a: 2.12 × 10^{-2}; b: 4.25 × 10^{-2}; c: 6.37 × 10^{-2}; d: 8.50 × 10^{-2}; e: 1.06 × 10^{-1}.

Table 4 Kinetic data for the complexes in DMF–H_2O at 30 ± 0.5 °C

Complex	x	b	k (mol $L^{-1})^{-2}$ s^{-1}
1	1.0527	−2.2581	0.14 × 10^3
2	1.0976	−2.11	0.19 × 10^3
3	1.0666	−1.6809	0.52 × 10^3
4	1.0967	−1.2923	1.28 × 10^3
5	0.9808	−1.5531	0.70 × 10^3

Conditions used: c(phosphate buffer) = 50 mmol L^{-1}, pH = 5.8, c(KBr) = 0.4 mol L^{-1}, c(phenol red) = 10^{-4} mol L^{-1}. "x" is the reaction order of the oxidovanadium complex; "b" is the intercept of the line; "k" is the reaction rate constant for the oxidovanadium complex.

The cyclic catalytic brominated reaction mechanism is shown in Scheme 3, in which step a: the vanadium complex is easily oxidized to form an intermediate compound of $[VO(O_2)L]$ with H_2O_2 as an oxidation regent; step b: Br^- is oxidized rapidly by the $[VO(O_2)L]$, while at the same time Br^+ and $[VO_2L]$ are formed. The catalytic reaction rate would be mainly based on the stability of the formed intermediate compound $[VO(O_2)L]$ (from step a to b).[55] The experimental results show that the order of the catalytic activity is **4** > **5** > **3** > **2** > **1**. This is because the formation of the intermediate compound $[VO(O_2)L]$ could be influenced by the different molecular structures of the complexes. The catalytic reaction activity of the complexes may correspond to the different molecular structures. Hereinto, the catalytic activity of complexes **4** and **5** with L^3 and L^4 are higher than those of complexes **1**, **2** and **3** with L^1 and L^2, which is explained by the fact that pyridine–pyrazole complexes form intermediate species more easily than triazine–pyrazole complexes.

Furthermore, comparisons of the kinetic data for the complexes reported previously are listed in Table 5. The order of the reaction rate constant for them is **9** > **4** > **6** > **10** > **5** > **3** > **7** > **8** > **2** > **1**. Complexes **6–10** were synthesized according to their corresponding references.[56–58] **6** is an oxidovanadium complex with a poly(pyrazole)borate ligand, **7** and **8** are oxidovanadium complexes with Schiff base ligands, while **9** and **10** are oxidovanadium complexes with a 2,2′-pyridine and 1,10-phenanthroline ligand, respectively. It is found that the catalytic activities of **1** and **2** are low, which may be due to the fact that the conjugated structure of the triazine ligands makes the complexes more stable and the formation of the intermediate peroxidovanadium $[VO(O_2)L]$ more difficult. The catalytic activity of complex **3** is higher than that of **1** and **2**, which is because the structure of **3** is a binuclear complex. The complexes with coordinated H_2O molecules all indicate higher catalytic activity, such as complexes **4**, **9** and **10**, which is attributed to the lower bond energy of the V–O single bond, resulting in the easier formation of the intermediate species $[VO(O_2)L]$, and among them, the conjugation behavior of the ligand in the complexes is **10** > **4** > **9**, so the order of the reaction rate constant is **9** > **4** > **10**. Compared with **5** and **6**, owing to the carboxylate group

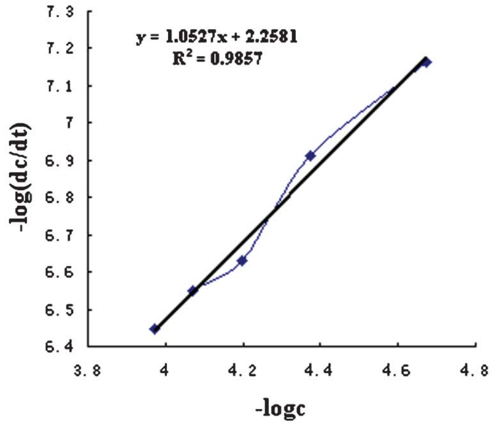

Fig. 9 −log(dc/dt) dependence of −log$c$ for **1** in DMF–H_2O at 30 ± 0.5 °C (c is the concentration of complex **1**; conditions used: c(phosphate buffer) = 50 mmol L^{-1}, pH = 5.8, c(KBr) = 0.4 mol L^{-1}, c(phenol red) = 10^{-4} mol L^{-1}.

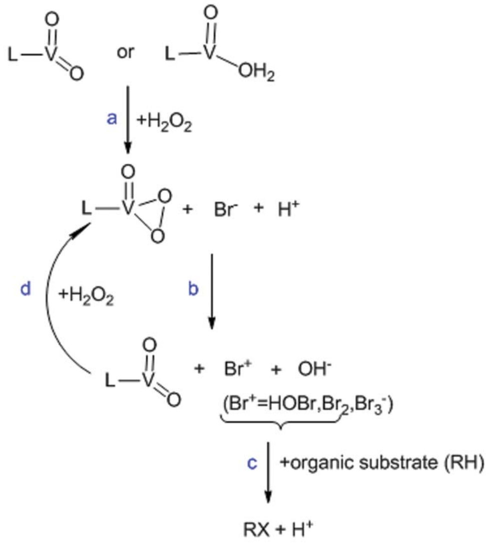

Scheme 3 The cyclic catalytic brominated reaction mechanism.

Table 5 Comparison of the kinetic data for the complexes in DMF–H_2O at 30 ± 0.5 °C

Complex	m	b	k (mol L^{-1})$^{-2}$ s^{-1}	Reference
1	1.0527	−2.2581	0.14 × 10^3	This work
2	1.0976	−2.11	0.19 × 10^3	This work
3	1.0666	−1.6809	0.52 × 10^3	This work
4	1.0967	−1.2923	1.275 × 10^3	This work
5	0.9808	−1.5531	0.699 × 10^3	This work
6[a]	1.0076	−2.3524	1.116 × 10^3	42
7[b]	0.9986	−2.7355	0.462 × 10^3	43
8[c]	1.02	−2.7758	0.421 × 10^3	43
9[d]	1.1153	−1.1672	2.347 × 10^3	44
10[e]	0.9921	−1.4858	1.003 × 10^3	44

[a] **6**: $VO(HB(3,5\text{-}Me_2pz)_3)(3,5\text{-}Me_2pz)(HOOCCH_2CH_2COO)$. [b] **7**: [VO(sal-ala)(2,2′-bipy)]·H_2O. [c] **8**: [VO(sal-ala)(1,10-phen)]·0.5H_2O. [d] **9**: $[VO(C_2O_4)(2,2'\text{-bipy})(H_2O)]\cdot C_2H_5OH$. [e] **10**: $[VO(C_2O_4)(phen)]\cdot H_2O$ (H_2sal-ala: Schiff base derived from salicylaldehyde and DL-α-alanine).

in **6** adopting a monodentate mode, it is easier for the intermediate species of the peroxidovanadium to form and the cleavage of the peroxide bond is easier, so the catalytic activity of complex **6** is higher.

Conclusions

In this work, five new complexes, supported by pincer-*N*-heterocyclic ligands, have been successfully synthesized for the first time. X-ray analysis reveals that the molecules in complexes, **2**, **3** and **5** form 1D chain structures, respectively, and that complex **1** forms a 2D sheet structure *via* intra- or intermolecular hydrogen bonds. However, two adjacent molecules in complexes **4** and **5** generate supermolecular structural dimers through intermolecular hydrogen bonds and the dimers could form a 1D and 3D structure *via* other intermolecular hydrogen bonding interactions, respectively. To explore more efficacious model oxovanadium complexes with the active centre of VHPO, we tested the bromination reaction activity with phenol red as an organic substrate in the presence of H_2O_2, KBr and a phosphate buffer solution, and complexes **4** and **5**, with L^3 or L^4 pincer *N*-heterocyclic ligands, have a higher catalytic activity than complexes **1**, **2** and **3**.

Acknowledgements

This work was supported by the grants of the National Natural Science Foundation of China (No. 21071071) and the State key Laboratory of Inorganic Synthesis and Preparative Chemistry, College of Chemistry, Jilin University, Changchun 130012, P. R. China (Grant No. 2013-05).

References

1 E. Lodyga-Chruscinska, G. Micera and E. Garribba, *Inorg. Chem.*, 2011, **50**, 883–899.

2 C. Wikete, P. Wu, G. Zampella, L. D. Gioia, G. Licini and D. Rehder, *Inorg. Chem.*, 2007, **46**, 196–207.

3 W. Plass, *Coord. Chem. Rev.*, 2011, **255**, 2378–2387.

4 F. Marchetti, C. Pettinari, C. D. Nicola, R. Pettinari, A. Crispini, M. Crucianelli and A. D. Giuseppe, *Appl. Catal., A*, 2010, **378**, 211–220.

5 M. R. Maurya, S. Agarwal, C. Bader and D. Rehder, *Eur. J. Inorg. Chem.*, 2005, 147–157.

6 I. Lippold, K. Vlay, H. Gorls and W. Plass, *J. Inorg. Biochem.*, 2009, **103**, 480–486.

7 T. F. S. Silva, K. V. Luzyanin, M. V. Kirillova, M. F. G. Da Silva, L. M. D. R. S. Martins and A. J. L. Pomberio, *Adv. Synth. Catal.*, 2010, **352**, 171–187.

8 (*a*) K. Kawabe, T. Sasagawa, Y. Yoshikawa, A. Ichimura, K. Kumekawa, N. Yanagihara, T. Takino, H. Sakurai and Y. Kojima, *J. Inorg. Biochem.*, 2003, **8**, 893–906; (*b*) Y. Shechter, I. Goldwaser, M. Mironchik, M. Fridkin and D. Gefel, *Coord. Chem. Rev.*, 2003, **237**, 3–11; (*c*) Y. Adachi, J. Yoshida, Y. Kodera, A. Katoh, J. Takada and H. Sakurai, *J. Med. Chem.*, 2006, **49**, 3251–3256; (*d*) M. J. Xie, X. D. Yang, W. P. Liu, S. P. Yan and Z. H. Meng, *J. Inorg. Biochem.*, 2010, **104**, 851–857.

9 (*a*) S. Karmaker, T. K. Saha, Y. Yoshikawa, H. Yasui and H. Sakurai, *J. Inorg. Biochem.*, 2006, **100**, 1535–1546; (*b*) T. Kiss, T. Jakusch, D. Hollender, Á. Dörnyei, É. A. Enyedy, J. C. Pessoa, H. Sakurai and A. Sanz-Medel, *Coord. Chem. Rev.*, 2008, **252**, 1153–1162; (*c*) A. A. Nejo, G. A. Kolawole, A. R. Opoku, J. Wolowska and P. O'brien, *Inorg. Chim. Acta*, 2009, **362**, 3993–4001; (*d*) K. H. Thompson and C. Orvig, *J. Inorg. Biochem.*, 2006, **100**, 1925–1935.

10 (*a*) V. Conte, A. Coletti, B. Floris, G. Licini and C. Zonta, *Coord. Chem. Rev.*, 2011, **255**, 2165–2177; (*b*) G. Romanowski and M. Wera, *Polyhedron*, 2010, **29**, 2747–2754.

11 (*a*) A. G. J. Ligtenbarg, R. Hage and B. L. Feringa, *Coord. Chem. Rev.*, 2003, **237**, 89–101; (*b*) G. Santoni and D. Rehder, *J. Inorg. Biochem.*, 2004, **98**, 758–764; (*c*) D. Rehder, *Inorg. Chem. Commun.*, 2003, **6**, 604–617.

12 (*a*) D. Rehder, *Coord. Chem. Rev.*, 1999, **182**, 297–322; (*b*) A. Pohlmann, S. Nica, T. K. K. Luong and W. Plass, *Inorg. Chem. Commun.*, 2005, **8**, 289–292; (*c*) A. Butler, *Curr. Opin. Chem. Biol.*, 1998, **2**, 279–285.

13 (*a*) G. E. M. Winter and A. Butler, *Biochemistry*, 1996, **35**, 11805–11811; (*b*) V. Conte, O. Bortolini, M. Carraro and S. Moro, *J. Inorg. Biochem.*, 2000, **80**, 41–49; (*c*) Y. H. Xing, K. Aoki, F. Y. Bai, Y. H. Zhang and B. L. Zhang, *J. Chem. Crystallogr.*, 2008, **38**, 327–331.

14 (*a*) R. C. Maurya, D. Sutradhar, M. H. Martin, S. R. J. Chourasia, A. K. Sharma and P. Vishwakarma, *Arabian J. Chem.*, 2012, DOI: 10.1016/j.arabjc.2011.01.009; (*b*) K. H. Thompson and C. Orvig, *Coord. Chem. Rev.*, 2001, **219–221**, 1033–1053; (*c*) M. J. Xie, Y. F. Niu, X. D. Yang, W. P. Liu, L. Li, L. H. Gao, S. P. Yan and Z. H. Meng, *Eur. J. Med. Chem.*, 2010, **45**, 6077–6084; (*d*) N. Teshima, M. Kuno, M. Ueda, H. Ueda, S. Ohno and T. Sakai, *Talanta*, 2009, **79**, 517–522; (*e*) M. T. Cocco, V. Onnis, G. Ponticelli, B. Meier, D. Rehder, E. Garribba and G. Micera, *J. Inorg. Biochem.*, 2007, **101**, 19–29.

15 (*a*) A. S. Tracey, G. R. Willsky and E. S. Takeuchi, *Vanadium Chemistry, Biochemistry Pharmacology and Practical Applications*, Taylor and Francis Group, Boca Raton, USA,

2007; (*b*) Y. Shechter, I. Goldwaser, M. Mironchik, M. Fridkin and D. Gefel, *Coord. Chem. Rev.*, 2003, **237**, 3–11; (*c*) H. Sakurai, Y. Yoshikawa and H. Yasui, *Chem. Soc. Rev.*, 2008, **37**, 2383–2392; (*d*) D. A. Barrio and S. B. Etcheverry, *Curr. Med. Chem.*, 2010, **17**, 3632–3642; (*e*) A. M. Evangelou, *Crit. Rev. Oncol. Hematol.*, 2002, **42**, 249–265; (*f*) A. Bishayee, A. Waghray, M. A. Patel and M. Chatterjee, *Cancer Lett.*, 2010, **294**, 1–12; (*g*) B. Mukherjee, B. Patra, S. Mahapatra, P. Banerjee, A. Tiwari and M. Chatterjee, *Toxicol. Lett.*, 2004, **150**, 135–143.

16 D. C. Crans, J. J. Smee, E. Gaidamauskas and L. Yang, *Chem. Rev.*, 2004, **104**, 849–902.

17 S. David, V. Barros, C. Cruz and R. Delgado, *FEMS Microbiol. Lett.*, 2005, **251**, 119–124.

18 (*a*) N. Mizuno and K. Kamata, *Coord. Chem. Rev.*, 2011, **255**, 2358–2370; (*b*) C. J. Schneider, J. E. Penner-Hahn and V. L. Pecoraro, *J. Am. Chem. Soc.*, 2008, **130**, 2712–2713.

19 S. Macedo-Ribeiro, R. Renirie, R. Wever and A. Messerschmidt, *Biochemistry*, 2008, **47**, 929–934.

20 (*a*) S. Rayati, A. Wojtczak and A. Kozakiewicz, *Inorg. Chim. Acta*, 2008, **361**, 1530–1533; (*b*) E. Kwiatkowski, G. Romanowski, W. Nowicki, M. Kwiatkowski and K. Suwinska, *Polyhedron*, 2007, **26**, 2559–2568; (*c*) G. Romanowski, E. Kwiatkowski, W. Nowicki, M. Kwiatkowski and T. Lis, *Polyhedron*, 2008, **27**, 1601–1609; (*d*) P. Plitt, H. Pritzkow and R. Kramer, *Dalton Trans.*, 2004, 2314–2320; (*e*) S. Mondal, M. Mukherjee, K. Dhara, S. Ghosh, J. Ratha, P. Banerjee and A. K. Mukherjee, *Cryst. Growth Des.*, 2007, **7**, 1716–1721.

21 (*a*) Y. H. Xing, K. Aoki, Z. Sun, M. F. Ge and S. Y. Niu, *J. Chem. Res.*, 2007, 108–114; (*b*) Y. H. Xing, B. L. Zhang, Y. H. Zhang, H. Q. Yuan, Z. Sun and M. F. Ge, *Polyhedron*, 2007, **26**, 3037–3044; (*c*) Y. H. Xing, F. Y. Bai, K. Aoki, Z. Sun and M. F. Ge, *Synth. React. Inorg., Met.-Org., Nano-Met. Chem.*, 2007, **37**, 203–211.

22 D. Wischang, O. Brücher and J. Hartung, *Coord. Chem. Rev.*, 2011, **255**, 2204–2217.

23 (*a*) M. A. Halcrow, *Coord. Chem. Rev.*, 2005, **249**, 2880–2908; (*b*) A. T. Baker, D. C. Craig and G. Dong, *Inorg. Chem.*, 1996, **35**, 1091–1092; (*c*) L. X. Xiao, Y. M. Luo, Z. Chen, J. Li and R. R. Tang, *Spectrochim. Acta, Part A*, 2008, **71**, 321–325.

24 (*a*) D. Quiñonero, P. M. Deyà, M. P. Carranza, A. M. Rodríguez, F. A. Jalón and B. R. Manzano, *Dalton Trans.*, 2010, **39**, 794–964; (*b*) H. P. Zhou, X. P. Gan, X. L. Li, W. Q. Geng, F. X. Zhou, W. Z. Ke, P. Wang, L. Kong, F. Y. Hao, J. Y. Wu and Y. P. Tian, *Cryst. Growth Des.*, 2010, **10**, 1767–1776; (*c*) S. N. Mikhaylichenko, S. M. Patel, S. Dalili, A. A. Chesnyuk and V. N. Zaplishny, *Tetrahedron Lett.*, 2009, **50**, 2505–2508.

25 Y. Q. Weng, M. L. Cao and B. H. Ye, *Inorg. Chem. Commun.*, 2011, **14**, 243–246.

26 (*a*) Y. Zhou and W. J. C. C. Chen, *Dalton Trans.*, 2007, 5123–5125; (*b*) Y. Zhou, W. Chen and D. J. C. C. Wang, *Dalton Trans.*, 2008, 1444–1453; (*c*) B. Zhao, H. Shu, H. Hu, T. Qin and X. Chen, *J. Coord. Chem.*, 2009, **62**, 1025–103.

27 A. Guerrero, F. A. Jalon, B. R. Manzano, R. M. Claramunt, P. Cabildo and L. Infantes, *Chem. Heterocycl. Compd.*, 2003, **39**, 1396–1403.

28 D. L. Comins and S. O'Connor, *Adv. Heterocycl. Chem.*, 1988, **44**, 199–267.

29 Y. Luo, Z. Chen, R. Tang and L. Xiao, *Chem. React. Eng. Technol.*, 2006, **22**, 549–553.

30 Y. Luo, L. Xiao, Z. Chen, W. Huang and X. Tang, *Chem. Res. Appl.*, 2008, **20**, 299–303.

31 G. M. Sheldrick, *SADABS, Program for Empirical AbsorptionCorrection for Area Detector Data*, University of Göttingen, Göttingen, Germany, 1996.

32 G. M. Sheldrick, *SHELXS 97, Program for Crystal Structure Refinement*, University of Göttingen, Göttingen, Germany, 1997.

33 B. Delley, *J. Chem. Phys.*, 1990, **92**, 508–517.

34 B. Delley, *J. Chem. Phys.*, 2000, **113**, 7756–7764.

35 M. Dolg, U. Wedig, H. Stoll and H. Preuss, *J. Chem. Phys.*, 1987, **86**, 866–872.

36 A. Bergner, M. Dolg, W. Kuechle, H. Stoll and H. Preuss, *Mol. Phys.*, 1993, **80**, 1431–1441.

37 J. P. Perdew, K. Burke and M. Ernzerhof, *Phys. Rev. Lett.*, 1997, **78**, 1396–1396.

38 P. Pulay, *J. Comput. Chem.*, 1982, **3**, 556–560.

39 R. S. Mulliken, *J. Chem. Phys.*, 1955, **23**, 1833–1846.

40 E. Verhaeghe, D. Buisson, E. Zekri, C. Leblanc, P. Potin and Y. Ambroise, *Anal. Biochem.*, 2008, **379**, 60–65.

41 C. Preiser, J. Loesel, I. D. Brown, M. Kunz and A. Skowron, *Acta Crystallogr., Sect. B: Struct. Sci.*, 1999, **55**, 698–711.

42 S. Adams, *Acta Crystallogr., Sect. B: Struct. Sci.*, 2001, **57**, 278–287.

43 A. Guerrero, F. A. Jalón, B. R. Manzano, A. Rodríguez, R. M. Claramunt, P. Cornago, V. Milata and J. Elguero, *Eur. J. Inorg. Chem.*, 2004, 549–556.

44 L. J. Wan, C. S. Zhang, Y. H. Xing, Z. Li, N. Xing, L. Y. Wan and H. Shan, *Inorg. Chem.*, 2012, **51**, 6517–6528.

45 H. Y. Zhao, F. Y. Bai, Y. H. Xing, Z. P. Li, Y. Z. Cao, X. Q. Zeng and M. F. Ge, *J. Coord. Chem.*, 2010, **63**, 435–447.

46 A. W. Addison, T. N. Rao, J. Reedijk, J. V. Rijn and G. C. Verschoor, *J. Chem. Soc., Dalton Trans.*, 1984, 1349–1356.

47 P. K. Chattaraj, D. R. Roy, M. Elango and V. Subramanian, *J. Phys. Chem. A*, 2005, **109**, 9590–9597.

48 J. Aihara, *J. Phys. Chem. A*, 1999, **103**, 7487–7495.

49 M. Yoshida and J. Aihara, *Phys. Chem. Chem. Phys.*, 1999, **1**, 227–230.

50 R. I. Rosa, M. J. Clague and A. Butler, *J. Am. Chem. Soc.*, 1992, **114**, 760–761.

51 M. R. Maurya, S. Agarwal, C. Bader, M. Ebel and D. Rehder, *Dalton Trans.*, 2005, 537–544.

52 M. R. Maurya, A. Kumar, M. Ebel and D. Rehder, *Inorg. Chem.*, 2006, **45**, 5924–5937.

53 T. N. Mandal, S. Roy, A. K. Barik, S. Gupta, R. J. Butcher and S. K. Kar, *Polyhedron*, 2008, **27**, 3267–3274.

54 A. Pohlmann, S. Nica, T. K. K. Luong and W. Plass, *Inorg. Chem. Commun.*, 2005, **8**, 289–292.

55 M. R. Maurya, A. Kumar, M. Ebel and D. Rehder, *Inorg. Chem.*, 2006, **45**, 5924–5937.

56 Y. Z. Cao, Z. P. Li, Y. H. Xing, D. M. Wei, Z. F. Pu, M. F. Ge and Z. Shi, *Chem. J. Chin. Univ.*, 2011, **32**, 1025–1032.

57 Y. Z. Cao, H. Y. Zhao, F. Y. Bai, Y. H. Xing, D. M. Wei, S. Y. Niu and Z. Shi, *Inorg. Chim. Acta*, 2011, **368**, 223–230.

58 D. X. Ren, Y. Z. Cao, C. Chen and Y. H. Xing, *Chem. Res. Chin. Univ.*, 2012, **28**(5), 768–774.